Ionic Liquid-Assisted Synthesis of Large-Scale TiO2 Nanoparticles with Controllable Phase by Hydrolysis of TiCl4

4 AUTHORS, INCLUDING:

Wenjun Zheng
Nankai University

112 PUBLICATIONS **2,284** CITATIONS

Lianjie Zhu
Tianjin University of Technology

25 PUBLICATIONS **289** CITATIONS

Ionic Liquid-Assisted Synthesis of Large-Scale TiO$_2$ Nanoparticles with Controllable Phase by Hydrolysis of TiCl$_4$

Wenjun Zheng,[†,]* Xiaodi Liu,[†] Zhiying Yan,[†] and Lianjie Zhu[‡]

[†]Department of Materials Chemistry, College of Chemistry, Nankai University, Tianjin 300071, People's Republic of China, and [‡]School of Chemistry and Chemical Engineering, Tianjin University of Technology, Tianjin 300191, People's Republic of China

ABSTRACT Pure rutile and rutile-anatase composite TiO$_2$ nanoparticles have been successfully synthesized *via* an ionic liquid-assisted method by hydrolysis of titanium tetrachloride in hydrochloric acid. It is found that the phase composition (ratio of rutile to anatase) of the products increases with increasing the content of ionic liquid [Emim]Br (1-ethyl-3-methyl-imidazolium bromide), therefore, TiO$_2$ nanoparticles with controlled phase compositions can be obtained in high yields. The structural and morphological characterizations of the resulting samples are investigated by means of X-ray powder diffraction (XRD), transmission electron microscopy (TEM), high-resolution TEM (HRTEM), and Brunauer−Emmett−Teller (BET) analysis, and the results indicate that the diameters of the anatase nanoparticles are in the range of 4−6 nm and the well-defined rutile nanorods are about 3−6 nm in diameter and 20−60 nm in length. More importantly, we find that the [Emim]$^+$ ions can serve as capping agents based on their strong interactions with the (110) facets of rutile, and the [Emim]Br favors the formation of the rutile structure with a rod-like shape due to the mutual π-stacking interactions of imidazole rings. We believe that this method can be developed into a general way to synthesize other metal oxide nanoparticles on a large scale.

KEYWORDS: nanostructures · rutile · rutile-anatase nanocomposite · ionic liquid · phase control

Nanostructure titanium dioxide (TiO$_2$), as a promising photocatalyst in photodegradations of most pollutants in water and air, has been extensively studied, mainly due to its superior ability of destruction of organic contaminants.[1,2] TiO$_2$ occurs mainly in three different polymorphs, which are anatase, rutile, and brookite, and it was reported that the phase composition of TiO$_2$ has effect on its photocatalytic property. Although the photocatalytic activity of rutile is still indistinct, several groups found that rutile phase shows higher photocatalytic activity than anatase, and a lot of experimental evidence supported that the existence of a synergistic effect between the anatase and rutile phases is beneficial for reducing the recombination of photogenerated electrons and holes, which usually results in an enhancement of photocatalytic activity.[3−7] However, it is known that anatase modification of TiO$_2$ can be obtained first in all solution synthesis pathways and it is even believed that anatase with particle size of 10−20 nm is a thermodynamically stable modification of TiO$_2$, when considering the contribution of surface energy.[8−10] More recently, rutile nanostructures have usually been synthesized *via* various solution routes. For instance, Aruna and co-workers have synthesized rutile nanocrystals from titanium isopropoxide in the presence of nitric acid *via* hydrothermal method. Wang *et al*. have presented a method to fabricate pure rutile nanocrystals by the thermohydrolysis of TiCl$_4$ in HCl-alcohol aqueous solution at 40−90 °C. Yang *et al*. have prepared rod-like and star-like rutile nanocrystals from TiCl$_4$/HCl solution by a sonochemical method.[11−18] However, in spite of the above successes, the ability to control the crystal structure and size of TiO$_2$ is still diffi-

cult in identifying suitable preparation processes. It should be mentioned that the formation of rutile is at the expense of anatase appeared in the early stage.[19] With regard to anatase-rutile composites, the synthesis of anatase-rich composite may be facile,[3,20−23] whereas the ability to control the phase ratio in rutile wealthy range still remains a challenge because the products usually grow into pure rutile phase rapidly.

Ionic liquids (ILs) have been widely studied as a new kind of reaction media owing to their unique properties such as extremely low volatility, wide liquid temperature range, good thermal stability, good dissolving ability, designable structures, high ionic conductivity, and wide electrochemical window.[24] Very recently, ILs have been used as solvents, reactants, or templates for the synthesis of inorganic nanomaterials with novel morphologies and improved properties.[25−27] As to TiO$_2$, the synthesis of highly crystalline anatase nanoparticles

TABLE 1. Preparation Conditions, Phase Contents, Crystalline Sizes, and BET Surface Areas of TiO₂

sample	[Emim]Br /mol · dm⁻³	anatase/%	rutile/%	crystalline size anatase/nm	crystalline size rutile/nm	S_{BET}/m² · g⁻¹
S-0	0	92		6.0		127
S-1	0.110	72.8	27.2	5.2	5.5	157
S-2	0.218	64.7	35.3	4.8	5.4	172
S-3	0.314	55.1	44.9	4.3	5.4	186
S-4	0.408	32.9	67.1	4.8	5.8	169
S-5	0.541	8.8	91.2	3.6	5.7	165
S-6	0.602	0	100		5.8	152

in ionic liquid media have been developed by some groups.[28−31] For example, anatase nanocrystals with uniform size and shape have been synthesized *via* a microwave-assisted route in IL. In addition, Kaper and co-workers have fabricated 148 × 3.8 nm rutile nanorods by an IL-assisted sol−gel reaction.[32] However, there is no report on the phase controlled synthesis of rutile-rich TiO₂ in IL, and it is still a challenge to explore a facile one-step route for the fabrication of high-quality rutile nanomaterials in this new kind of reaction medium.

ILs have already been proven to be an excellent media for the synthesis of inorganic materials. As a burgeoning field, clarifying the following two issues will be very important for future research. The first issue is how can the characteristics of ionic liquids, such as hydrogen-bonding, $\pi-\pi$ interaction, and molecular cluster, be applied to synthesize inorganic materials? The second issue is how can this novel synthesis technology be used to provide insight into potential synthesis mechanisms for many other materials?

Herein, we report a facile ionic liquid-assisted synthesis of pure rutile and rutile-anatase composite nanoparticles by hydrolysis of titanium tetrachloride in hydrochloric acid. The ionic liquid, [Emim]Br (1-ethyl-3-methyl-imidazolium bromide), can serve as a capping agent based on its strong interaction with the (110) facet of rutile. More specifically, we demonstrate that [Emim]Br favors the formation of rutile structure with a rod-like shape due to the mutual π-stacking of imidazole rings. The ratios of rutile to anatase in the products can be controlled and TiO₂ nanoparticles with arbitrary phase compositions can be obtained in high yields by means of this simple method.

RESULTS AND DISCUSSION

Structural Characterization, Morphology, and BET Analysis of TiO₂ Nanoparticles. The experiment was conducted in a water-[Emim]Br complex system containing hydrochloric acid and TiCl₄ at 100 °C for 24 h. Hydrochloric acid served as an acidic catalyst to control the hydrolysis speed of titanium source and its concentration was set to 6 mol · dm⁻³. The ratios of rutile to anatase in the products could be controlled by changing the concentrations of [Emim]Br in the system. The detailed reaction conditions were listed in Table 1.

As shown in Figure 1, the X-ray powder diffraction (XRD) patterns illustrate the crystalline phase evolution of TiO₂ synthesized in the presence of [Emim]Br with different concentrations. In the absence of [Emim]Br, anatase with minor amounts of brookite is formed. Brookite disappears with the addition of [Emim]Br and, instead, rutile appears. Increasing the concentration of [Emim]Br leads to further growth of rutile phase, and the product (S-6) is close to pure rutile structure in about 0.602 mol · dm⁻³ [Emim]Br. The Raman spectrum of S-6 exhibits four absorption bands at 141, 247, 442, and 605 cm⁻¹, which are in good agreement with the characteristic mode of the rutile phase,[33] therefore, it further confirms the XRD result (see Figure S1 in the Supporting Information). The relative phase percentages of TiO₂ can be routinely appraised as a function of XRD peak areas of different crystallographic forms (anatase and rutile), based on the following equations[34]

$$W_A = K_A I_A / (K_A I_A + I_R)(K_A = 0.886)$$

$$W_R = I_R / (K_A I_A + I_R)$$

where W_A and W_R are the weight fraction of anatase and rutile and I_A and I_R are obtained from the peak areas of anatase (101) and rutile (110) diffractions, respectively. Accordingly, the phase contents of anatase and
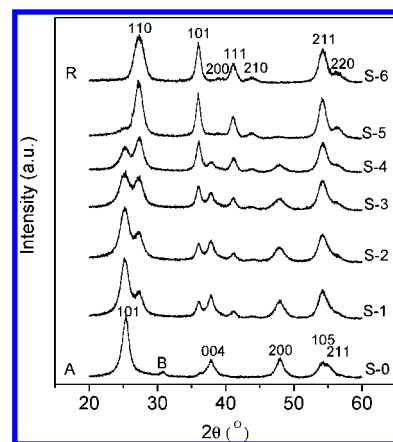

Figure 1. XRD patterns of TiO₂ synthesized with different concentrations of [Emim]Br. (S-0) 0; (S-1) 0.110; (S-2) 0.218; (S-3) 0.314; (S-4) 0.408; (S-5) 0.541; (S-6) 0.602 mol · dm⁻³. A, B, and R represent anatase, brookite, and rutile, respectively.
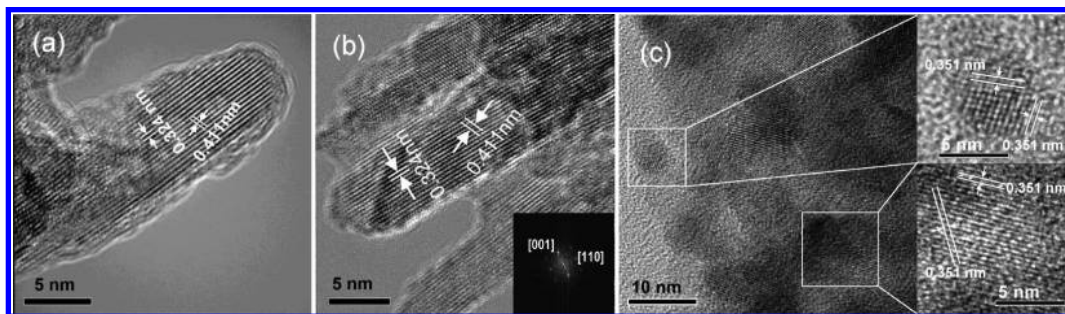
Figure 2. (a−c) HRTEM images of three samples corresponding to S-5 (a), S-6 (b), and S-0 (c), respectively. The inset of (b) is the corresponding fast Fourier transform (FFT) pattern, which takes along the [−110] zone axis.

rutile in the products synthesized with different contents of [Emim]Br are calculated and listed in Table 1. It can be found from the results that the rutile phase content almost linearly changes with the concentration of [Emim]Br in the range of 0−0.602 mol·dm^{-3}. These results indicate that the rutile content can be controlled by simply varying the concentration of [Emim]Br. Moreover, the average crystallize sizes of anatase and rutile in the samples are calculated by employing Debye−Scherrer formula based on the anatase (101) and rutile (110) diffraction peaks, and the results are tabulated in Table 1. We also estimate the surface areas (S_{BET}) of the samples by BET method (shown in Table 1). It is found that the S_{BET} shows high value in the range from 120 to 180 m^2·g^{-1}, and the S_{BET} increases at the beginning but intends to decrease with further increasing the rutile content. In addition, the results of C, H, N elemental analysis display that no [Emim]Br obviously resides at the samples after washing with distilled water and anhydrous alcohol for several times.

As confirmed by the XRD pattern of rutile phase, the half-peak breadth of (110) reflection is distinctly larger than that of (101) reflection, which suggests that the rutile structure is oriented-growth. We investigate the TEM images of the samples synthesized with different contents of [Emim]Br. Figure S2a−d show the TEM images of S-0, S-2, S-5, and S-6, respectively (see the

Supporting Information). S-0 mainly contains about 4−6 nm cube-like nanoparticles, whereas S-2 and S-5 consist of both rod-like and cube-like nanoparticles. Well-defined rod-shaped nanoparticles in 3−6 nm diameter range are found in S-6 and their lengths are in the range of 20−60 nm. Moreover, the rutile structure grows into the main phase and the rod-like nanoparticles become the dominant component, which suggests that the cube-like particles are anatase and the rod-like ones are rutile. As shown in Figure 2a-c, the HRTEM images of samples S-0, S-5, and S-6 can further substantiate this suggestion. For rutile particles, (1−10) and (1−20) planes can be determined by the approximate 72° interfacial angle and the d-spacing of 0.324 and 2 × 0.205 nm, respectively. The growing processes have made the rutile (110) surface occupy a dominant exposed plane (Figure 2a,b); moreover, the [001] direction, the preponderant growth direction, agrees with the equilibrium shape of a crystal in the rutile phase.[35,36] Two kinds of two dimension lattice fringes are observed in anatase particles, which agrees with the truncated bipyramid shape (Figure 2c). The shape and crystal planes of this bipyramid-shaped particle is similar to the equilibrium shape of a anatase crystal,[28,29,35] whereas preponderant growth direction is not obviously observed.
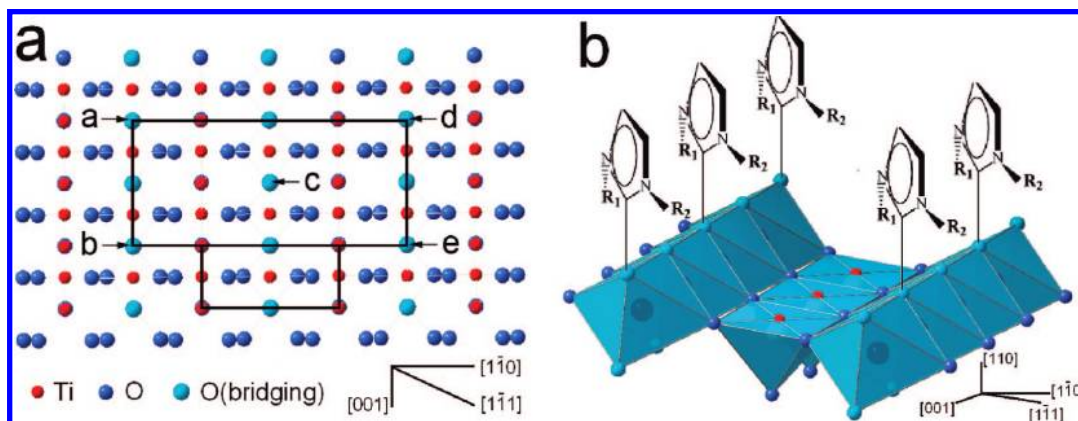
Scheme 1. (a) Surface structure of rutile cleaved along the [110] direction and schematic illustration of rutile (110)-c(2×2)-[Emim]$^+$ original cell, moreover, [Emim]$^+$ ions locate in the a−e sites, whereas [Emim]$^+$ units are omitted for clarity. The large and small rectangles represent the original cell and rutile cell, respectively. (b) Schematic illustration of a projected view of [Emim]$^+$ ions anchored onto rutile (110) plane to form tight coverage layer *via* the original cell.
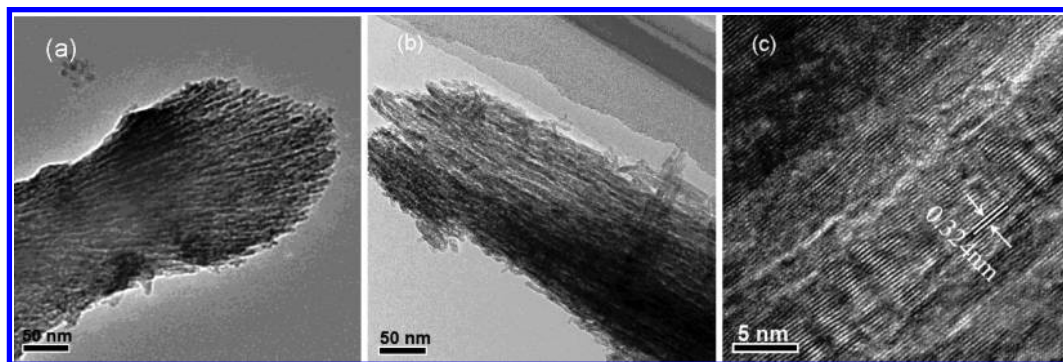
Figure 3. (a) TEM image of rutile prepared from the medium with 0.1 mol·dm^{-3} [Bmim]Br. (b,c) TEM and HRTEM images of rutile prepared from the medium with 0.05 mol·dm^{-3} [C$_{16}$mim]Br.

Effect of [Emim]Br on the Structure and Morphology of TiO$_2$.
According to the results mentioned above, it is found that the [Emim]Br play a critical role in the controlling the crystal structure and morphology of TiO$_2$ nanoparticles. As demonstrated by Bahnemann *et al.*,[37] which because of surface acidic and basic properties, positive charge can absorb on TiO$_2$ surface when pH < 3.5, adsorbing competition between H$^+$ and [Emim]$^+$ ions will then be considered. Although H$^+$ ion presents higher electrostatic effect and Lewis acidity, [Emim]$^+$ ion may be have more preference for adsorbing on the TiO$_2$ surface, at least in the second half of the reaction process as HCl and water gradually volatilizing form the system at reaction temperature. Besides electrostatic interactions, three other factors can be identified for the adsorption of [Emim]$^+$ ion. The first factor makes a point of a large steric hindrance of [Emim]$^+$ ion, which would hinder the diffusion of H$^+$ ions toward the TiO$_2$ surface; the second one is based on the mutual π-stacking interaction between aromatic rings; and the last influencing factor is the hydrogen-bonding interaction existing in the O(rutile surface)−H−C([Emim]$^+$ rings), because the H atoms in C2 position of [Emim]$^+$ rings present Lewis acidity.[38]

Some authors have reported that on TiO$_2$ surfaces, the possible adsorption configuration of anatase (101) plane is very similar to that of rutile (110) plane.[39] Consequently, the fact that [Emim]Br favors the formation of rutile structure may be due to the different structures of anatase (101) and rutile (110) planes. The structure of rutile (110) plane is believed to be very close to the bulk truncated geometry and the most stable crystal face.[35,36] In this way, the (110) plane unit cell contains one 2-fold coordinated bridging O atom above the (110) truncated plane. The distances between bridging O atoms along [001], [1−10] and [1−11] directions are 0.296, 0.650, and 0.714 nm, respectively. As shown in Scheme 1a, if [Emim]$^+$ ions vertically adsorbed on the (110) plane *via* a rutile(110)-c(2×2)-[Emim]$^+$ original cell (Scheme 1a), the space between [Emim]$^+$ ions along [001] direction is duplicate d_{001}-spacing (0.592 nm). Fortunately, in various directions, the [Emim]$^+$ ions are separated in accordance with the mutual π-stacking

distance (0.6−0.7 nm) between the aromatic rings.[40,41] Consequently, we suggest that [Emim]$^+$ ions can be allowed to anchor onto rutile (110) plane to form relatively tight coverage layer (Scheme 1b). In comparison with rutile (110) plane, anatase (101) plane is also the most thermodynamically stable plane of anatase, however, this plane is toothed and the distance between bridging O atoms is not in the space range of the mutual π-stacking between aromatic rings. Therefore, it is impossible for [Emim]$^+$ ions to perpendicularly adsorb on the anatase (101) plane and construct a tight coverage layer. Among the usual crystal planes of anatase, none of them is suitable for forming coverage layer by this [Emim]$^+$ ion adsorbing model (see Figure S3 in the Supporting Information). This discussion expounded that rutile phase is the more favorable oriented growth at a relatively high initial concentration of [Emim]Br.

In order to confirm the above discussions, two experiments were carried out. First, the obtained pure rutile (S-6) was added into the same synthetic condition, except that the concentration of HCl was selected as 6 and 2 mol·dm^{-3}, respectively (the details were described in the Supporting Information). After adsorbing, the samples were adjusted to FT-IR measurements. The adsorption bands at 1571, 1618, and 1168 cm^{-1} (see Figure S4 in the Supporting Information) belong to the imidazole ring skeleton stretching vibration;[42,43] the adsorption bands at 3152 and 3099 cm^{-1} are assigned to the stretching vibration of C(2)-H in an imidazole ring, become round and weak, which can attribute to the strong hydrogen bonding interaction formed between the C([Emim]$^+$)−H-O(TiO$_2$).[44] Although, as compared with 2 mol·dm^{-3} HCl, the adsorption bands of hydrogen bonding for 6 mol·dm^{-3} HCl are weaker to some extent, [Emim]$^+$ ions can adsorb on the TiO$_2$ surface and form hydrogen bonds between [Emim]$^+$ and TiO$_2$ surface.

In addition, if the explanations for the mechanism of effect of [Emim]Br on the structure of TiO$_2$ (shown in Scheme 1) are reasonable, the structure-directing effect of ionic liquid on the rutile is closely related to its ability to self-assemble in ordered structures. It has been reported that the self-assembled ability of

imidazole-based ionic liquid is affected by the length of alkyl chain at the 1-position of its cation.[45] In our experiments, [Bmim]Br (1-butyl-3-methyl-imidazolium bromide) and [C_{16}mim]Br (1-hexadecyl-3-methyl-imidazolium bromide) are also used to synthesize TiO_2 nanoparticles. The XRD results indicate that in the two synthetic systems, pure rutile can be obtained as the concentration of [Bmim]Br and [C_{16}mim]Br is reached to 0.1 and 0.05 mol·dm^{-3}, respectively (see Figure S5 in the Supporting Information). The morphologies of the as-prepared two samples are investigated by TEM. Figure 3 shows the typical TEM and HRTEM images of the rutile synthesized in [Bmim]Br and [C_{16}mim]Br. Figure 3a shows that the rutile prepared in [Bmim]Br consisted of nanorods, whose diameters are about 6 nm and lengths are more than 100 nm. Figure 3b and c are the TEM and HRTEM images of the rutile synthesized in the [C_{16}mim]Br. It also can be found that the lengths of the rutile nanorods are increased with the increasing of the alkyl chain length (Figure 3b). Moreover, the HRTEM image of a typical nanorods is shown in Figure 3c, from which one can see that the lattice spacing is 0.324 nm, corresponding to the (110) plane of rutile. Therefore, the [001] direction is the preponderant growth direction, which is consistent with the S-6. Based on the above discussions, it can be speculated that self-assembled ability of ionic liquids has prominent influence on the structural orientation of rutile. Therefore, the adsorption model (Scheme 1) can rationally explain the influence of ionic liquid on the structure and morphology of the product. In order to control the phase compositions (ratio of rutile to anatase) of the products, furthermore, considering that [Emim]Br has good solubility in water and anhydrous ethanol and can be easily washed form the products, we therefore employed [Emim]Br in the synthetic system.

Possible Formation Mechanism of TiO_2 Nanoparticles with Controlled Phase Composition. It has been reported that anatase formed in early stage can be converted into rutile.[19] To investigate the phase evolution of the TiO_2, time-dependent experiments were carried out and the
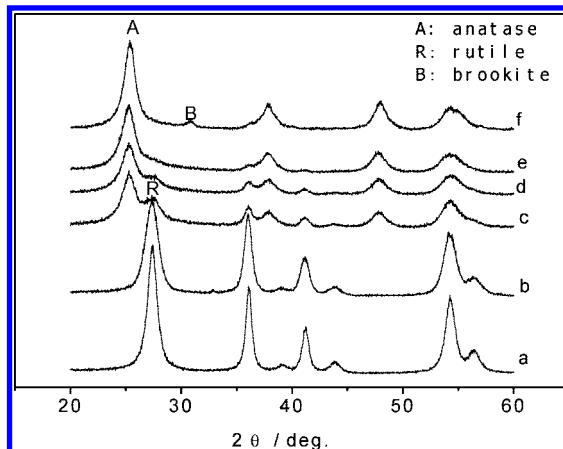
Figure 4. XRD patterns of TiO_2 nanoparticles synthesized with different concentrations of HCl in the absence of [Emim]Br: (a) 1, (b) 2, (c) 3, (d) 4, (e) 5, (f) 6 mol·dm^{-3}.

resulting products collected at different reaction times were analyzed by XRD. As shown in Figure S6 (see the Supporting Information), when the reaction time was 12 h, anatase was observed as the main phase, whereas rutile with minor anatase existed in the sample at 15 h. These results indicated that the formation of rutile is still at the expense of anatase appeared in the early stages.

We found that the concentration of HCl has influence on the phase component of the as-synthesized TiO_2 (see Figure S7 in the Supporting Information). In fact, such a 6 mol·dm^{-3} HCl solution is more than required to construct pure rutile nanoparticles. When the concentration of HCl is increased, the anatase as a coexistent phase appears in the product, further increasing the concentration, moreover, results in a distinct increasing of anatase phase. To further study the effect of HCl concentration, a series of control experiments in the absence of [Emim]Br have been performed by changing the concentrations of HCl from 1 mol·dm^{-3} to 2, 3, 4, and 5 mol·dm^{-3}. The XRD results, shown in Figure 4, display a similar evolution tendency of crystal structure and indicate that the rutile and anatase phases can meet with each other when the concentration of HCl is *ca.* 3 mol·dm^{-3}.
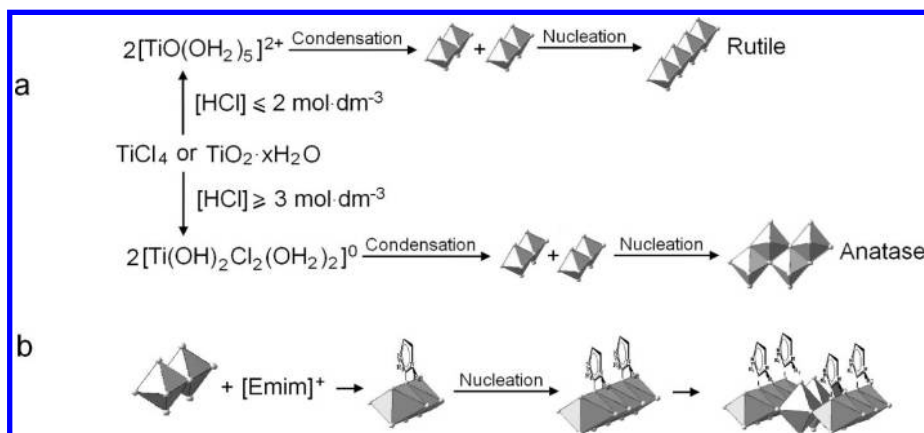
Scheme 2. Illustration of the nucleation pathways that lead to TiO_2 nanocomposites with different rutile contents: (a) with different concentrations of HCl without [Emim]Br, (b) in the present of [Emim]Br.
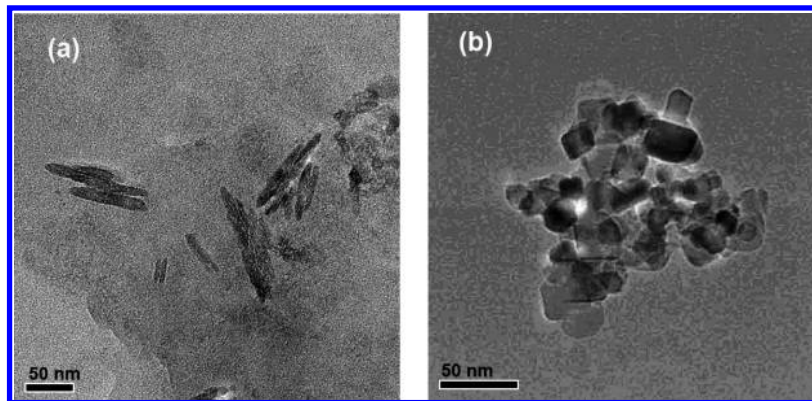
Figure 5. TEM images of rutile nanoparticles synthesized in 1 mol·dm^{-3} HCl: (a) with 0.218 mol·dm^{-3} [Emim]Br; (b) without [Emim]Br.

In addition, besides the concentration of HCl, the content of [Emim]Br also play an important role in controlling the phase component of the final product. In a given initial concentration of HCl, the content of [Emim]Br will become the only decisive factor for the phase component. As discussed above, the change in rutile content of samples shows a nearly linear relation with the content of [Emim]Br. At the beginning, anatase structure is favored, anatase phase, therefore, predominates in the products. The HCl gradually volatilizes from the system with increasing the reaction time, at the same time rutile structure appears and grows at the expense of anatase. When the concentration of HCl is decreased to a given threshold value, the reaction must be terminated to ensure the presence of anatase in the final products. On the basis of the above experimental results, it is reasonable to believe that the [Emim]Br and HCl have cooperative effects on the phase composition of TiO$_2$ nanoparticles, and we propose the possible formation mechanism of TiO$_2$ nanoparticles with controlled phase composition (Scheme 2).

As shown in previous studies by others, when [HCl] $\leq$ 2 mol·dm^{-3}, [TiO(OH$_2$)$_5$]$^{2+}$ monomer becomes predominant in a TiCl$_4$ solution with low concentration, which is prone to condense *via* olation. In this way, only edge-sharing linear nuclei can be formed, which leads to the rutile phase (Scheme 2a).[46,47] If [HCl] $\geq$ 3 mol·dm^{-3}, an intermediate species, [Ti(OH)$_2$Cl$_2$(OH$_2$)$_2$]^0 seems to be dominant and will then combine with each other to form anatase phase (Scheme 2a).[48]

Generally, the crystal growth of TiO$_2$ in acidic medium can be explained as follows:[12,49,50] discrete TiO$_6$ octahedra form Ti-OH$_2$$^+$ *via* protonation of Ti-OH groups, and then these protonated octahedra are easy to combine with -OH groups of other TiO$_6$ octahedra to con-

struct Ti−O−Ti oxygen bridge bonds by eliminating a water molecule. For a given acidity, if [Emim]$^+$ ion is allowed to substitute H$^+$ ion, the consequence will be that [Emim]−O-Ti group and related species favor the linear nuclei *via* edge-sharing TiO$_6$ octahedra based on the mutual π-stacking between aromatic rings (Scheme 2b). Others have already found the direct interaction between imidazolium-type ionic liquids and TiO$_6$ octahedra in synthesized process.[31,32] The interaction between [Emim]$^+$ and TiO$_6$ octahedra could be a decisive factor for the formation of rutile phase due to the spatial effect, which is beneficial for the catenarian nuclei *via* edge-sharing polycondensation between TiO$_6$ octahedra. It has also been shown by chelation of citrate to TiO$_6$ octahedra that edge-sharing chain is favored for nucleation process.[31,32] Besides the effect of controlling the structure, as a template, [Emim]Br can also strengthen the oriented-growth habit of rutile structure. When the concentration of HCl and [Emim]Br are 1 and 0.218 mol·dm^{-3}, respectively, as shown in Figure 5a, rutile nanorods with $(3-5) \times (10-50)$ nm can be successfully synthesized; however, cube-like nanoparticles with *ca.* 25 nm are obtained without employing [Emim]Br (Figure 5b). These results can be regarded as evidence to further confirm the existence of interactions between [Emim]$^+$ and TiO$_6$ octahedra and the rationality of the mutual π-stacking between aromatic rings.

CONCLUSIONS

In summary, pure rutile and rutile-anatase nanocomposites have been successfully synthesized by hydrolysis of titanium tetrachloride in hydrochloric acid with the assistance of [Emim]Br. The content of rutile in the composites can be controlled by simply adjusting the amount of [Emim]Br added to the synthetic system. According to this approach, the composites with arbitrary content of rutile have been rationally and reproducibly prepared in high yields. This method has following obvious advantages: The process is simple; The reaction can be performed under atmospheric pressure in a glass vessel, and no high-pressure and high temperature apparatus is needed; Products are highly crystalline and their components are controllable. We believe that this method can be developed into a general way to synthesize other metal oxide nanoparticles on a large scale.

METHODS

Synthesis of TiO$_2$ Nanoparticles. In a typical synthesis of TiO$_2$ nanoparticles, 1 mL of pure titanium tetrachloride was added dropwise to 50 mL of hydrochloric acid, and the concentration of the acid was 6 mol·dm^{-3}. The final titanium concentration in the mixtures was 0.15 mol·dm^{-3}. Different amounts of [Emim]Br

was added to the above solution, and then the solution was transferred into a glass beaker. Thereafter, the solutions were heated and aged at 100 °C for 24 h in an oven. The product was separated by centrifugation, washed with distilled water and anhydrous ethanol for several times.

Instruments and Characterizations. XRD measurements were performed on a Rigaku D/max 2500 diffractometer with Cu Kα radia-

tion (λ = 0.154056 nm) at 40 kV and 120 mA, using a nickel filter. TEM and HRTEM images were recorded with a Tecnai G^2 20 S-Twin transmission electron microscope operating at an accelerating voltage of 120 and 200 kV, respectively. Raman spectra were measured in the frequency range 80–4000 cm^{-1} using Bruker RFS-100 FT-Raman spectrometer using the 1064 nm wavelength of an argon laser with 500 mW power as an excitation source. The N$_2$ adsorption measurements were carried out at −196 °C after drying in vacuum at 100 °C on a CHEMBET-3000, and the BET surface areas of the samples were calculated using the BET (Brunauer−Emmett−Teller) equation. The elemental analyses were performed on Elementar-Vorio EL CHN analyzer. The FT-IR spectra were recorded from KBr tablets in the region of 4000−1000 cm^{-1} on a Nicolet Magna 560 spectrometer.

Supporting Information Available: Additional experimental details and results. This material is available free of charge *via* the Internet at http://pubs.acs.org.

REFERENCES AND NOTES

1. Hoffmann, M. R.; Martin, S. T.; Choi, W.; Bahnemann, D. W. Environmental Applications of Semiconductor Photocatalysis. *Chem. Rev.* **1995**, *95*, 69–96.
2. Jiang, D.; Zhang, S.; Zhao, H. Photocatalytic Degradation Characteristics of Different Organic Compounds at TiO$_2$ Nanoporous Film Electrodes with Mixed Anatase/Rutile Phases. *Environ. Sci. Technol.* **2007**, *41*, 303–308.
3. Bacsa, R. R.; Kiwi, J. Effect of Rutile Phase on the Photocatalytic Properties of Nanocrystalline Titania during the Degradation of *p*-Coumaric Acid. *Appl. Catal., B* **1998**, *16*, 19–29.
4. Mills, A.; Lee, S. K.; Lepre, A. Photodecomposition of Ozone Sensitised by a Film of Titanium Dioxide on Glass. *J. Photochem. Photobiol. A* **2003**, *155*, 199–205.
5. Watson, S.; Beydoun, D.; Scott, J.; Amal, R. R. Preparation of Nanosized Crystalline TiO$_2$ Particles at Low Temperatures for Photocatalysis. *J. Nanopart. Res.* **2004**, *6*, 193–207.
6. Yan, M. C.; Chen, F.; Zhang, J.; Anpo, M. Preparation of Controllable Crystalline Titania and Study on the Photocatalytic Properties. *J. Phys. Chem. B* **2005**, *109*, 8673–8678.
7. Gumy, D.; Morais, C.; Bowen, P.; Pulgarin, C.; Giraldo, S.; Hajdu, R.; Kiwi, J. Catalytic Activity of Commercial of TiO$_2$ Powders for the Abatement of the Bacteria (*E. coli*) under Solar Simulated Light: Influence of the Isoelectric Point. *Appl. Catal., B* **2006**, *63*, 76–84.
8. Zhang, H.; Banfield, J. F. Thermodynamic Analysis of Phase Stability of Nanocrystalline Titania. *J. Mater. Chem.* **1998**, *8*, 2073–2076.
9. Barnard, A. S.; Curtiss, L. A. Prediction of TiO$_2$ Nanoparticle Phase and Shape Transitions Controlled by Surface Chemistry. *Nano Lett.* **2005**, *5*, 1261–1266.
10. García, M. F.; Wang, X.; Belver, C.; Hanson, J. C.; Rodriguez, J. A. Anatase-TiO$_2$ Nanomaterials: Morphological/Size Dependence of the Crystallization and Phase Behavior Phenomena. *J. Phys. Chem. C* **2007**, *111*, 674–682.
11. Cheng, H.; Ma, J.; Zhao, Z.; Qi, L. Hydrothermal Preparation of Uniform Nanosize Rutile and Anatase Particles. *Chem. Mater.* **1995**, *7*, 663–671.
12. Yanagisawa, K.; Ovenstone, J. Crystallization of Anatase from Amorphous Titania Using the Hydrothermal Technique: Effects of Starting Material and Temperature. *J. Phys. Chem. B* **1999**, *103*, 7781–7787.
13. Fei, B.; Deng, Z. X.; Xin, J. H.; Zhang, Y. H.; Pang, G. Room Temperature Synthesis of Rutile Nanorods and Their Applications on Cloth. *Nanotechnology* **2006**, *17*, 1927–1931.
14. Aruna, S. T.; Tirosh, S.; Zaban, A. Nanosize Rutile Titania Particle Synthesis *via* a Hydrothermal Method without Minerizers. *J. Mater. Chem.* **2000**, *10*, 2388–2391.
15. Pal, M.; Serrano, J. G.; Santiago, P.; Pal, U. Size-Controlled Synthesis of TiO$_2$ Nanoparticles: Morphology, Crystallization, and Phase Transition. *J. Phys. Chem. C* **2007**, *111*, 96–102.
16. Wang, W.; Gu, B. H.; Liang, L. Y.; Hamilton, W. A.; Wesolowski, D. J. Synthesis of Rutile(α-TiO$_2$) Nanocrystals with Controlled Size and Shape by Low-Temperature Hydrolysis: Effects of Solvent Composition. *J. Phys. Chem. B* **2004**, *108*, 14789–14792.
17. Wang, Y. W.; Zhang, L. Z.; Deng, K. J.; Chen, X. Y.; Zou, Z. G. Low Temperature Synthesis and Photocatalytic Activity of Rutile TiO$_2$ Nanorod Superstructures. *J. Phys. Chem. C* **2007**, *111*, 2709–2714.
18. Yang, K.; Zhu, J. M.; Zhu, J. J.; Huang, S. S.; Zhu, X. H.; Ma, G. B. Sonochemical Synthesis and Microstructure Investigation of Rod-like Nanocrystalline Rutile Titania. *Mater. Lett.* **2003**, *57*, 4639–4642.
19. Jolivet, J. P.; Henry, M.; Livage, J. *Metal Oxide Chemistry and Synthesis*; John Wiley & Sons, Ltd.: Chichester, 2000; p 82.
20. Yu, J. C.; Yu, J.; Ho, W.; Zhang, L. Preparation of Highly Photocatalytic Active Nano-sized TiO$_2$ Particles *via* Ultrasonic Irradiation. *Chem. Commun.* **2001**, 1942–1943.
21. Abe, R.; Sayama, K.; Arakawa, H. Significant Influence of Solvent on Hydrogen Production from Aqueous I^{3-}/I$^-$ Redox Solution Using Dye-sensitized Pt/TiO$_2$ Photocatalyst under Visible Light Irradiation. *Chem. Phys. Lett.* **2003**, *379*, 230–235.
22. Ohno, T.; Tokieda, K.; Higashida, S.; Matsumura, M. Synergism between Rutile and Anatase TiO$_2$ Particles in Photocatalytic Oxidation of Naphthalene. *Appl. Catal., A* **2003**, *244*, 383–391.
23. Testino, A.; Bellobono, I. R.; Buscaglia, V.; Canevali, C.; Arienzo, M. D.; Polizzi, S.; Scotti, R.; Morazzoni, F. Optimizing the Photocatalytic Properties of Hydrothermal TiO$_2$ by the Control of Phase Composition and Particle Morphology. *J. Am. Chem. Soc.* **2007**, *129*, 3564–3575.
24. Antonietti, M.; Kuang, D. B.; Smarsly, B.; Zhou, Y. Ionic Liquids for the Convenient Synthesis of Functional Nanoparticles and Other Inorganic Nanostructure. *Angew. Chem., Int. Ed.* **2004**, *43*, 4988–4992.
25. Parnham, E. R.; Morris, R. E. Ionothermal Synthesis Using a Hydrophobic Ionic Liquid as Solvent in the Preparation of a Novel Aluminophosphate Chain Structure. *J. Mater. Chem.* **2006**, *16*, 3682–3684.
26. Taubert, A. CuCl Nanoplatelets from an Ionic Liquid-Crystal Precursor. *Angew. Chem., Int. Ed.* **2004**, *43*, 5380–5382.
27. Lin, Z.; Wragg, D. S.; Morris, R. E. Microwave-Assisted Synthesis of Anionic Metal-Organic Frameworks under Ionothermal Conditions. *Chem. Commun.* **2006**, 2021–2023.
28. Zhou, Y.; Antonietti, M. Synthesis of Very Small TiO$_2$ Nanocrystals in a Room-Temperature Ionic Liquid and Their Self-Assembly toward Mesoporous Spherical Aggregates. *J. Am. Chem. Soc.* **2003**, *125*, 14960–14961.
29. Nakashima, T.; Kimizuka, N. Interfacial Synthesis of Hollow TiO$_2$ Microspheres in Ionic Liquids. *J. Am. Chem. Soc.* **2003**, *125*, 6386–6387.
30. Liu, Y.; Li, J.; Wang, M. J.; Li, Z. Y.; Liu, H. T.; He, P.; Yang, X. R.; Li, J. H. Preparation and Properties of Nanostructure Anatase TiO$_2$ Monoliths Using 1-butyl-3-methylimidazolium Tetrafluoro-borate Room-Temperature Ionic Liquids as Template Solvents. *Cryst. Growth Des.* **2005**, *5*, 1643–1649.
31. Ding, K. L.; Miao, Z. J.; Liu, Z. M.; Zhang, Z. F.; Han, B. X.; An, G. M.; Miao, S. D.; Xie, Y. Facile Synthesis of High Quality TiO$_2$ Nanocrystals in Ionic Liquid *via* a Microwave-Assisted Process. *J. Am. Chem. Soc.* **2007**, *129*, 6362–6363.
32. Kaper, H.; Endres, F.; Djerdj, I.; Antonietti, M.; Smarsly, B. M.; Maier, J.; Hu, Y. S. Direct Low-Temperature Synthesis of Rutile Nanostructures in Ionic Liquid. *Small* **2007**, *10*, 1753–1763.
33. Melendres, C. A.; Narayanasamy, A.; Maroni, V. A.; Siegel, R. W. Raman Spectroscopy of Nanophase TiO$_2$ Source. *J. Mater. Res.* **1989**, *4*, 1246–1250.

34. Zhang, H.; Banfield, J. F. Understanding Polymorphic Phase Transformation Behavior during Growth of Nanocrystalline Aggregates: Insights from TiO_2. *J. Phys. Chem. B* **2000**, *104*, 3481–3487.

35. Diebold, U. The Surface Science of Titanium Dioxide. *Surf. Sci. Rep.* **2003**, *48*, 53–229.

36. Bullock, B. L.; Patthey, L.; Steinemann, S. G. Clean and Hydroxylated Rutile TiO_2 (110) Surfaces Studied by X-ray Photoelectron Spectroscopy. *Surf. Sci.* **1996**, *352−354*, 504–510.

37. Bahnemann, D.; Henglein, A.; Spanhel, L. Detection of the Intermediates of Colloidal TiO_2-Catalysed Photoreactions. *Faraday Discuss. Chem. Soc.* **1984**, *78*, 151–163.

38. Dong, K.; Zhang, S. J.; Wang, D. X.; Yao, X. Q. Hydrogen Bonds in Imidazolium Ionic Liquids. *J. Phys. Chem. A* **2006**, *110*, 9775–9782.

39. Chang, J. G.; Wang, J. H.; Lin, M. C. Adsorption Configurations and Energetics of BCl_x ($x = 0−3$) on TiO_2 Anatase (101) and Rutile (110) Surfaces. *J. Phys. Chem. A* **2007**, *111*, 6746–6754.

40. Yaghi, O. M.; Li, G. M.; Li, H. L. Selective Binding and Removal of Guests in a Microporous Metal-Organic Framework. *Nature* **1995**, *378*, 703–706.

41. Jin, J.; Iyoda, T.; Cao, C.; Song, Y.; Jiang, L.; Li, T.; Zhu, D. Self-Assembly of Uniform Spherical Aggregates of Magnetic Nanoparticles through $\pi−\pi$ Interactions. *Angew. Chem., Int. Ed.* **2001**, *40*, 2135–2138.

42. Hu, Y.; Liu, Y. J.; Yu, J. Y.; Xu, Y. P.; Tian, Z. J.; Lin, L. W. Ionothermal Synthesis of Aluminophosphate Molecular Sieve. *Chin. J. Inorg. Chem.* **2006**, *22*, 753–756.

43. Zhu, J. M.; Shen, Y. H.; Xie, A. J.; Qiu, L. G.; Zhang, Q.; Zhang, S. Y. Photoinduced Synthesis of Anisotropic Gold Nanoparticles in Room-Temperature Ionic Liquid. *J. Phys. Chem. C* **2007**, *111*, 7629–7633.

44. Wang, L.; Chang, L. X.; Zhao, B.; Yuan, Z. Y.; Shao, G. S.; Zheng, W. J. Systematic Investigation on Morphologies, Forming Mechanism, Photocatalytic and Photoluminescent Properties of ZnO Nanostructures Constructed in Ionic Liquids. *Inorg. Chem.* **2008**, *47*, 1443–1452.

45. Bowlas, C. J.; Bruce, D. W.; Seddon, K. R. Liquid-Crystalline Ionic Liquids. *Chem. Commun.* **1996**, 1625–1626.

46. Zheng, Y. Q.; Shi, E. W.; Chen, Z. Z.; Li, W. J.; Hu, X. F. Influence of Solution Concentration on the Hydrothermal Preparation of Titania Crystallites. *J. Mater. Chem.* **2001**, *11*, 1547–1551.

47. Henry, M.; Jolivert, J. P.; Livage, J. *Structure and Bonding*; Springer-Verlag: Berlin, 1992; Vol. 77, p 155.

48. Pottier, A.; Chanéac, C.; Tronc, E.; Mazerolles, L.; Jolivet, J. P. Synthesis of Brookite TiO_2 Nanoparticles by Thermolysis of $TiCl_4$ in Strongly Acidic Aqueous Media. *J. Mater. Chem.* **2001**, *11*, 1116–1121.

49. Brinker, C. J.; Scherer, G. W. *Sol-Gel Science: The Physics and Chemistry of Sol-Gel Processing*; Academic Press: New York, 1990; p 240.

50. Yin, H. B.; Wada, Y.; Kitamura, T.; Kambe, S.; Murasawa, S.; Mori, H.; Sakatac, T.; Yanagida, S. Hydrothemal Synthesis of Nanosized Anatase and Rutile TiO_2 Using Amorphous Phase TiO_2. *J. Mater. Chem.* **2001**, *11*, 1694–1703.